ISSN 1674-1056
http://cpb.iphy.ac.cn
http://iopscience.iop.org/cpb
中国物理 B
Chinese Physics
中国物理
Chinese Physics B

Formation mechanism of asymmetric breather and rogue waves in pair-transition-coupled nonlinear Schrödinger equations

Zai-Dong Li(李再东), Yang-yang Wang(王洋洋), Peng-Bin He(贺鹏斌)

Citation: Chin. Phys. B . 2019, 28(1): 010504. **doi:** 10.1088/1674-1056/28/1/010504
Journal homepage: http://cpb.iphy.ac.cn; http://iopscience.iop.org/cpb

What follows is a list of articles you may be interested in

Symmetry and asymmetry rogue waves in two-component coupled nonlinear Schrödinger equations

Zai-Dong Li(李再东), Cong-Zhe Huo(霍丛哲), Qiu-Yan Li(李秋艳), Peng-Bin He(贺鹏斌), Tian-Fu Xu(徐天赋)
Chin. Phys. B . 2018, 27(4): 040505. **doi:** 10.1088/1674-1056/27/4/040505

Soliton structures in the (1+1)-dimensional Ginzburg-Landau equation with a parity-time-symmetric potential in ultrafast optics

Wenyi Li(李文义), Guoli Ma(马国利), Weitian Yu(于维天), Yujia Zhang(张玉佳), Mengli Liu(刘孟丽), Chunyu Yang(杨春玉), Wenjun Liu(刘文军)
Chin. Phys. B . 2018, 27(3): 030504. **doi:** 10.1088/1674-1056/27/3/030504

Controllable optical superregular breathers in the femtosecond regime

Yang Ren(任杨), Zhan-Ying Yang(杨战营), Chong Liu(刘冲), Wen-Li Yang(杨文力)
Chin. Phys. B . 2018, 27(1): 010504. **doi:** 10.1088/1674-1056/27/1/010504

Asymmetric W-shaped and M-shaped soliton pulse generated from a weak modulation in an exponential dispersion decreasing fiber

Xiang-Shu Liu(刘祥树), Li-Chen Zhao(赵立臣), Liang Duan(段亮), Zhan-Ying Yang(杨战营), Wen-Li Yang(杨文力)
Chin. Phys. B . 2017, 26(12): 120503. **doi:** 10.1088/1674-1056/26/12/120503

Analytical solutions and rogue waves in (3+1)-dimensional nonlinear Schrödinger equation

Ma Zheng-Yi,Ma Song-Hua
Chin. Phys. B . 2012, 21(3): 030507. **doi:** 10.1088/1674-1056/21/3/030507

Formation mechanism of asymmetric breather and rogue waves in pair-transition-coupled nonlinear Schrödinger equations*

Zai-Dong Li(李再东)[1,2,†], Yang-yang Wang(王洋洋)[1], and Peng-Bin He(贺鹏斌)[3]

[1] *Department of Applied Physics, Hebei University of Technology, Tianjin* 300401, *China*

[2] *Key Laboratory of Electronic Materials and Devices of Tianjin, School of Electronics and Information Engineering, Hebei University of Technology, Tianjin* 300401, *China*

[3] *School of Physics and Electronics, Hunan University, Changsha* 410082, *China*

(Received 25 September 2018; revised manuscript received 6 November 2018; published online 27 December 2018)

Based on the developed Darboux transformation, we investigate the exact asymmetric solutions of breather and rogue waves in pair-transition-coupled nonlinear Schrödinger equations. As an example, some types of exact breather solutions are given analytically by adjusting the parameters. Moreover, the interesting fundamental problem is to clarify the formation mechanism of asymmetry breather solutions and how the particle number and energy exchange between the background and soliton ultimately form the breather solutions. Our results also show that the formation mechanism from breather to rogue wave arises from the transformation from the periodic total exchange into the temporal local property.

Keywords: Akhmediev breather solution, Kuznetsov–Ma breather solution, rogue wave, nonuniform exchange

PACS: 05.45.Yv, 42.65.Tg **DOI:** 10.1088/1674-1056/28/1/010504

1. Introduction

In the 1960s, the nonlinear models began to emerge. At the same time, the development of nonlinear science in this context became an important discipline. With the rapid development of science and technology, Hasegawa derived the nonlinear Schrödinger (NLS) equation[1] from the dispersion equation of nonlinear terms in 1973, which plays a very important role in the related sciences, such as nonlinear wave dynamics[2] and others.[3,4] So far, the NLS equation has been widely used in the fields of optics,[5] water tanks,[6–8] Bose–Einstein condensates,[9–11] hydrodynamics,[12] plasma physics,[13–16] molecular biology,[17] magnetic nanowires[18–20] driven by spin-polarized current,[21–23], and even finance.[24,25] Famous physicists Benney and Newell proposed coupled NLS (CNLS) equations 30 years ago, which quickly became another important nonlinear physical model. Many physical phenomena usually have more than one component.[26–31] Furthermore, in practical physics, the number of particles in each component is not necessarily conserved. These systems are usually non-integrable. It is not easy to study nonlinear systems; therefore, the research of integrable CNLS equations is very meaningful. Manakov obtained bright solitons in the focusing medium by backscattering[32] and proved the integrability of CNLS equations. For the nonzero background, there are many studies for CNLS equations.[33–41] Some nonlinear models of integrable CNLS equations are obtained on the basis of the special Hirota bilinearization and the Darboux transformation,[42–44] such as those used in solitons,[45–49] breathers,[50,51] and rogue waves.[18–20,52–56] The soliton is an isolated wave that still maintains its original velocity and shape after interaction. The breather is a special localized-in-space oscillating solution, mainly due to the instability of the small amplitude disturbance, and the solution has periodicity in the temporal or spatial direction. The common breathers are the Akhmediev breather and Kuznetsov–Ma solution, which are mainly in the form of hyperbolic functions. The Akhmediev breather has been studied for a long time, and was confirmed in numerical experiments in 2009.[51] The particular class of solution exhibiting Fermi–Pasta–Ulam-like growth–return evolution is now widely referred to within the fluid dynamics community as the Akhmediev breather. It is excited by weak periodic modulation and is limited to longitudinal dimensions when experiencing growth and decay. The Kuznetsov–Ma soliton was confirmed in 2012.[17] The rogue waves were first discovered in the ocean,[57] and its theoretical research began in 1965. Professors Akhmediev and Pelinovsky discussed the definition of rogue waves with researchers of many fields.[58] Scientists who participated in the discussion have expressed their own opinions of rogue waves, but there is not a complete and accurate definition of rogue waves. Generally, the amplitude of the rogue waves can reach more than twice the chaotic amplitude in the region around the rogue wave packet. Rogue waves occur suddenly and are localized in time-space.[59,60] The main results focus on the formation of these nonlinear

*Project supported by the National Natural Science Foundation of China (Grant No. 61774001) and the Natural Science Foundation of Hunan Province, China (Grant No. 2017JJ2045).

†Corresponding author. E-mail: lizd@hebut.edu.cn

© 2019 Chinese Physical Society and IOP Publishing Ltd

solutions, while little research has been presented on their formation mechanism.

In this paper, we mainly investigate the exact analytical breather solutions and rogue waves of the CNLS equations. Under certain specific parameters, we can get two types of breather solutions, i.e., Kuznetsov–Ma breather solutions and Akhmediev breather solutions. We mainly investigate the propagation characteristics of asymmetric and symmetric Kuznetsov–Ma breather solutions and exact asymmetric Akhmediev breather solutions. Moreover, we focus on the formation mechanism of asymmetric breather solutions and how the particle number and energy exchange between the background and soliton ultimately form the breather solutions. It can be described by the total nonuniform exchange. We will also explore the formation mechanism from breather solutions to rogue wave.

2. Exact breather solution of CNLS equations

The CNLS equations with negative coherent coupling can describe the propagation of the orthogonally polarized optical waves in an isotropic medium. In the paraxial approximation, the CNLS equations take the form

$$\begin{aligned} &\mathrm{i}q_{1t}+q_{1xx}+2\left(|q_1|^2+2|q_2|^2\right)q_1-2q_1^*q_2^2=0,\\ &\mathrm{i}q_{2t}+q_{2xx}+2\left(|q_2|^2+2|q_1|^2\right)q_2-2q_2^*q_1^2=0, \end{aligned} \tag{1}$$

where q_1 and q_2 are the slowly varying envelopes of two interacting optical modes, with the asterisk being the complex conjugate. The variables x and t correspond to the normalized distance and retarded time, respectively. In Eq. (1), the coefficients of the self-phase modulation and the cross-phase modulation are different, and the last terms at the left-hand side are known as the coherent coupling term. In fact, equation (1) is an integrable model and its solutions can be obtained by the effective Darboux transformation method and Hirota bilinear method. Equation (1) is found to admit Lax pair

$$\begin{aligned} \Psi_x &= (\lambda U_0+U_1)\Psi,\\ \Psi_t &= \left(\lambda^2V_0+\lambda V_1+V_2\right)\Psi, \end{aligned} \tag{2}$$

in which the compatibility condition $\Psi_{xt}=\Psi_{tx}$ yields the CNLS in Eq. (1). Here, $U_0=\mathrm{i}\begin{pmatrix}-I_{2\times2} & O\\ O & I_{2\times2}\end{pmatrix}$, $U_1=\begin{pmatrix}O & Q\\ -Q^\dagger & O\end{pmatrix}$, $Q=\begin{pmatrix}q_1 & q_2\\ -q_2 & q_1\end{pmatrix}$, $V_0=\mathrm{diag}(-2\mathrm{i},-2\mathrm{i},2\mathrm{i},2\mathrm{i})$, $V_1=2\begin{pmatrix}O & Q\\ -Q^\dagger & O\end{pmatrix}$, $V_2=\mathrm{i}\begin{pmatrix}QQ^\dagger & Q_x\\ Q_x^\dagger & -Q^\dagger Q\end{pmatrix}$, $I_{2\times2}=\mathrm{diag}(1,1)$, and $\Psi=\begin{pmatrix}\varphi_1 & \varphi_2 & \varphi_3 & \varphi_4\\ -\varphi_2 & \varphi_1 & -\varphi_4 & \varphi_3\end{pmatrix}^{\mathrm{T}}$, where the superscript T signifies the matrix transpose, Ψ is the matrix eigenfunction, φ_j ($j=1$, 2, 3, and 4) is the function of x and t, $I_{2\times2}$ is the 2×2 unit matrix, O is the 2×2 zero matrix, † denotes the conjugate transpose, and λ is the eigenvalue parameter. If one assume that $\Psi=\begin{pmatrix}\varphi_1 & \varphi_2 & \varphi_3 & \varphi_4\\ -\varphi_2 & \varphi_1 & -\varphi_4 & \varphi_3\end{pmatrix}^{\mathrm{T}}$ is a solution of Eq. (2) corresponding to λ, then $\begin{pmatrix}-\varphi_3^* & \varphi_4^* & \varphi_1^* & -\varphi_2^*\\ \varphi_4^* & \varphi_3^* & -\varphi_2^* & -\varphi_1^*\end{pmatrix}^{\mathrm{T}}$ is also a solution of Eq. (2) corresponding to the eigenvalue λ^*.

In this paper, we adopt the Darboux transformation and mainly investigate the exact breather solutions and its formation mechanism. To this purpose, we choose the initial seed solutions of Eq. (1) as

$$q_n^{(0)}=a_n\mathrm{e}^{\mathrm{i}\phi_\mathrm{c}}, \tag{3}$$

which is a continuous wave (cw) solution, where $n=1$ and 2, $\phi_\mathrm{c}=kx-\omega t$, and the frequency ω satisfies the nonlinear dispersion relation $\omega=k^2-2\left(a_1^2+a_2^2\right)$. By employing the normal process of Darboux transformation and substituting Eq. (3) into Eq. (2), we obtain the corresponding eigenfunctions

$$\begin{aligned} \varphi_1 &= \mathrm{e}^{\mathrm{i}\phi_\mathrm{c}/2}\left(C_1\mathrm{e}^{A}+C_2\mathrm{e}^{-A}\right),\\ \varphi_2 &= \mathrm{e}^{\mathrm{i}\phi_\mathrm{c}/2}\left(C_3\mathrm{e}^{A}+C_4\mathrm{e}^{-A}\right),\\ \varphi_3 &= \mathrm{e}^{-\mathrm{i}\phi_\mathrm{c}/2}\left[\,\kappa_1\left(a_2C_3-a_1C_1\right)\mathrm{e}^{A}\right.\\ &\quad\left.+\kappa_2\left(a_2C_4-a_1C_2\right)\mathrm{e}^{-A}\,\right],\\ \varphi_4 &= -\mathrm{e}^{-\mathrm{i}\phi_\mathrm{c}/2}\left[\,\kappa_1\left(a_2C_1+a_1C_3\right)\mathrm{e}^{A}\right.\\ &\quad\left.+\kappa_2\left(a_2C_2+a_1C_4\right)\mathrm{e}^{-A}\,\right], \end{aligned} \tag{4}$$

where C_j ($j=1$, 2, 3, and 4) is a complex constant. Other parameters are given by

$$\begin{aligned} A &\equiv \theta+\mathrm{i}\varphi=\Xi\left(x+(2\lambda-k)t\right),\\ \Xi &= \sqrt{-(k/2+\lambda)^2-\left(a_1^2+a_2^2\right)},\\ \kappa_1 &= 1/\left(\Xi-\mathrm{i}k/2-\mathrm{i}\lambda\right),\\ \kappa_2 &= 1/\left(\kappa_1\left(a_1^2+a_2^2\right)\right), \end{aligned} \tag{5}$$

where $\lambda=\mu+i\nu$, and μ and ν are the real constants.

With the help of eigenfunctions in Eq. (4) and employing the standard process of the Darboux transformation, we have

$$q_n=q_n^{(0)}+4\nu\frac{f_n}{g}, \tag{6}$$

where $n=1$ and 2, and other parameters are defined by

$$\begin{aligned} f_1 &= \left(\varphi_1^2+\varphi_2^2\right)\left(\varphi_1^*\varphi_3^*+\varphi_2^*\varphi_4^*\right)\\ &\quad+\left(\varphi_3^{*2}+\varphi_4^{*2}\right)\left(\varphi_1\varphi_3+\varphi_2\varphi_4\right),\\ f_2 &= \left(\varphi_1^2+\varphi_2^2\right)\left(\varphi_1^*\varphi_4^*-\varphi_2^*\varphi_3^*\right)\\ &\quad+\left(\varphi_3^{*2}+\varphi_4^{*2}\right)\left(\varphi_1\varphi_4-\varphi_2\varphi_3\right),\\ g &= \sum_{j=1}^{4}\left|\varphi_j\right|^2+\left(\varphi_1\varphi_2^*-\varphi_2\varphi_1^*+\varphi_3\varphi_4^*-\varphi_4\varphi_3^*\right)^2. \end{aligned}$$

Equation (6) indicates the exact breather solutions of Eq. (1), which is combined with the exponential function dependence with temporal and spatial coordinates. We also see that the

exponential function's form can be determined by the parameters C_j, which ultimately affect the types of breather solutions, as shown in the following section. The very interesting fundamental problem is to investigate the formation mechanism of asymmetric breather solutions and the particle number and energy exchange between the background and soliton. Lastly, we will explore the formation mechanism from breather to rogue wave solutions.

3. Asymmetric and symmetric Kuznetsov–Ma breather solutions

From Eqs. (4), (5), and (6) we find that the wave number k of the initial seed solution contributes a velocity to the soliton propagation. Therefore, for the sake of brevity, we can only consider the case of $\mu = 0$ and $k = 0$ in the following discussion. When $\nu^2 > a_1^2 + a_2^2$, we obtain the Kuznetsov–Ma breather solutions of Eq. (6), which is characterized by the key parameters as follows:

$$\begin{aligned} \theta &= \Xi x,\ \varphi = 2\nu\Xi t, \\ \Xi &= \sqrt{\nu^2 - \left(a_1^2 + a_2^2\right)}, \\ \kappa_1 &= 1/\left(\Xi + \nu\right), \\ \kappa_2 &= 1/\left(\kappa_1\left(a_1^2 + a_2^2\right)\right). \end{aligned} \tag{7}$$

With the above parameters, we see that the main characteristic properties of breather solutions in Eq. (6) are spatially aperiodic and temporally periodic, which is denoted by the parameters in Eqs. (4) and (7). Therefore, this type of expression is usually called a Kuznetsov–Ma breather solution. It is obvious that under the cw background, the parameter C_j determines the type of Kuznetsov–Ma breather images, i.e. the component $|q_1|^2$ and $|q_2|^2$ are the same or different type of shape, which will be discussed in detail below.

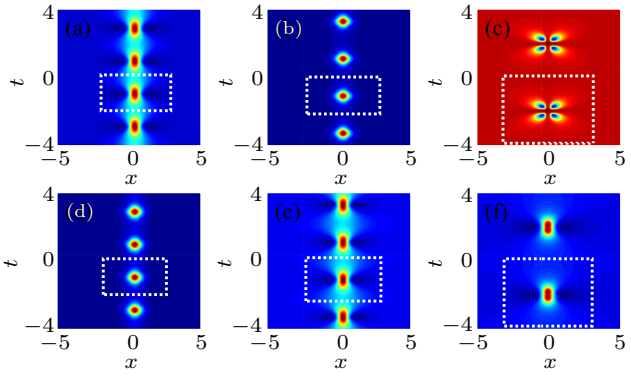


Fig. 1. Density plots of the Kuznetsov–Ma breather solution in Eq. (6) with specific values of $\nu = 1$, $C_1 = 1$, $C_2 = 0$, $C_3 = 3$, and $C_4 = 2$. The white boxes in the figure represent a period, as in the figures below. (a)–(c) Plots for the component $|q_1|^2$ and (d)–(f) plots for the component $|q_2|^2$. From each time period unit, it is seen that (a) has one peak and two valleys, and (d) has only one peak. Other parameters are as follows: (a) and (d) $a_1 = 0.59$, $a_2 = 0$; (b) and (e) $a_1 = 0$, $a_2 = 0.7055$; (c) and (f) $a_1 = 0.59$, $a_2 = 0.7055$.

Firstly, we assume $C_2 = 0$ and get the asymmetric Kuznetsov–Ma breather images, i.e. the component $|q_1|^2$ and $|q_2|^2$ share different types of shape, as shown in Fig. 1. From Figs. 1(a), 1(b), 1(d), and 1(e), we find that each seed cw solution ($q_1^{(0)} \neq 0$, $q_2^{(0)} = 0$, or $q_1^{(0)} = 0$, $q_2^{(0)} \neq 0$) brings into existence a bright Kuznetsov–Ma breather solution for two components. However, under the combined action of two seed cw and soliton solutions, the component q_1 takes the dark Kuznetsov–Ma breather with one peak and four valleys in each temporal periodic unit, while the other component q_2 still keeps two peaks and four valleys, as shown in Figs. 1(c) and 1(f), respectively.

In order to deeply investigate the properties of Kuznetsov–Ma breather solutions in Eq. (6), the analysis for the density distribution against the background plays a major role, which is defined by the quantity $\rho_n(x,t) = |q_n(x,t)|^2 - |q_n(x \to \pm\infty, t)|^2$, $n = 1$ and 2. For the existence of a single seed solution ($q_1^{(0)} \neq 0$, $q_2^{(0)} = 0$), the breather property of q_1 comes from two parts, i.e. the interaction between the cw solution and the soliton solution, as well as the coherent coupling term in Eq. (1). This implies that at a fixed time, the loss in background is transferred to the hump, and then it gathers energy from the background toward its central part, and vice versa. However, the same property of component q_2 is only determined by the coherent coupling term in Eq. (1). The same result occurs for the case of $q_1^{(0)} = 0$, $q_2^{(0)} \neq 0$. The other interesting fundamental problem is how breather solutions gather the particle number and energy toward its central part in each temporal periodic unit from the background. This can be explained by the local nonuniform exchange $\delta_n(x,t) \equiv \lim_{l_Q \to \pm\infty} |q_n(x,t) - q_n(x = l_Q, t)|^2$, and the total nonuniform exchange, i.e. the integral

$$\xi_n(t) = \int_{-\infty}^{+\infty} \delta_n(x,t)\,\mathrm{d}x. \tag{8}$$

With the existence of two seed cw solutions, the graphical illustration is given in Fig. 2 for the total exchange $\xi_n(t)$. For the existence of single seed solutions, the total nonuniform exchange of the two components q_1 and q_2 has periodic characteristics, as shown in Figs. 2(a) and 2(b). In each temporal periodic unit, the energy in the background first accumulates to the central part, and then dissipates into the background, which forms the generation of a hump and two valleys on the background along the space direction, as shown in Figs. 1(a), 1(b), 1(d), and 1(e). However, in the case of two seed cw solutions, there is cross interaction, i.e. the exchange between the cw background and soliton, and the coherent coupling effect between two components denoted in Eq. (1). The total exchange period for each component decreases with the increase in amplitudes a_1 and a_2 of two seed cw solutions. The component q_1 has four accumulations and dissipations, while the component q_2 has only two, as shown in Fig. 2.

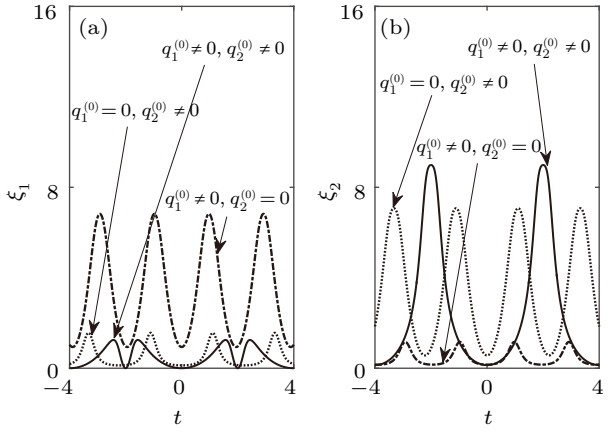


Fig. 2. The nonuniform exchange of the Kuznetsov–Ma breather solution in Eq. (8). (a) For ξ_1 and (b) for ξ_2. The parameters are $\nu = 1$, $C_1 = 1$, $C_2 = 0$, $C_3 = 3$, and $C_4 = 2$; $a_1 = 0.59$, $a_2 = 0$ (long dashed line); $a_1 = 0$, $a_2 = 0.7055$ (short dashed line); $a_1 = 0.59$, $a_2 = 0.7055$ (solid line).

Secondly, we further take into account the case of $C_2 = C_3 = 0$ and have the graphical illustration of q_1 and q_2 in Fig. 3 for the single and two seed solutions, respectively. From Figs. 3(a), 3(b), 3(d), and 3(e), we find that each seed solution ($q_1^{(0)} \neq 0$, $q_2^{(0)} = 0$, or $q_1^{(0)} = 0$, $q_2^{(0)} \neq 0$) brings into existence a dark Kuznetsov–Ma breather with four valleys for its own component in each temporal periodic unit, while the other component takes the bright Kuznetsov–Ma breather with two peaks and two valleys. However, under the combined action of two seed cw solutions and the soliton, the component q_1 has only one peak and one valley with a sub minimum, and four valleys in each temporal periodic unit. Meanwhile, the other component q_2 still keeps two peaks and two saddle points with different values, as shown in Figs. 3(c) and 3(f), respectively.

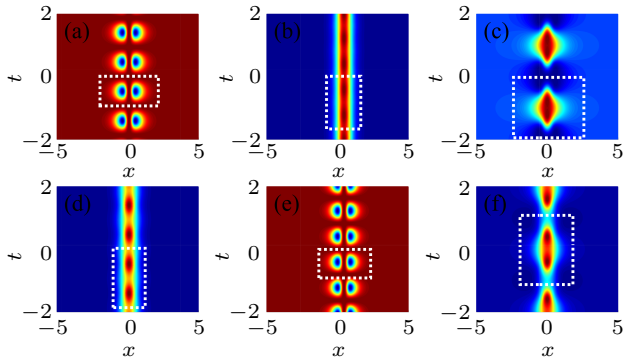


Fig. 3. The transmission of the Kuznetsov–Ma breather solution in Eq. (6). (a)–(c) Transmission for the component $|q_1|^2$ and (d)–(f) transmission for the component $|q_2|^2$. The parameters are $\nu = 1$, $C_1 = 1$, $C_2 = C_3 = 0$, and $C_4 = 0.35$; (a) and (d) $a_1 = 0.55$, $a_2 = 0$; (b) and (e) $a_1 = 0$, $a_2 = 0.284$; (c) and (f) $a_1 = 0.55$, $a_2 = 0.284$.

With the existence of two seed solutions, the graphical illustration is plotted in Fig. 4 for the total nonuniform exchange $\xi_n(t)$. From Fig. 4(a), we find that the energy in the background first accumulates to the central part, which leads to the generation of a hump on the background along the space direction, and the critical peak of the hump can occur for q_1. Then, the energy in the hump starts to dissipate into the background and tends to the opposite accumulation, which leads to two valleys and one valley with a sub minimum in each temporal periodic unit, as shown in Fig. 3(c). The same law of total nonuniform exchange shown in Fig. 4(b) can only result in two valleys and one valley with a sub minimum for the component q_2 in Fig. 3(f).

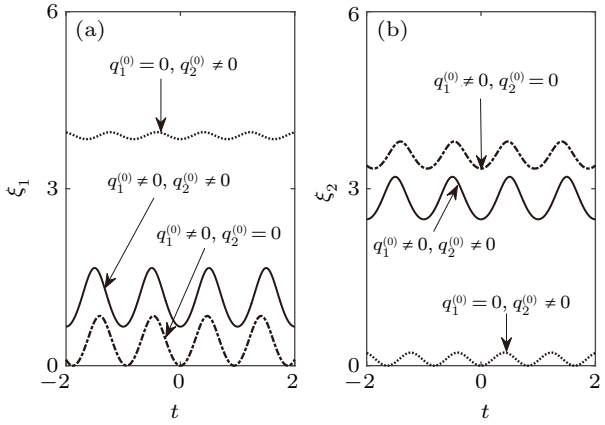


Fig. 4. The nonuniform exchange of the Kuznetsov–Ma breather solution in Eq. (8). (a) For ξ_1 and (b) for ξ_2. The parameters are $\nu = 1$, $C_1 = 1$, $C_2 = C_3 = 0$, and $C_4 = 0.35$; $a_1 = 0.55$, $a_2 = 0.284$ (solid line); $a_1 = 0$, $a_2 = 0.284$ (short dashed line); $a_1 = 0.55$, $a_2 = 0$ (long dashed line).

At last, we consider the case of $C_3 = C_4 = 0$ and obtain the symmetric Kuznetsov–Ma breather images, i.e. the components $|q_1|^2$ and $|q_2|^2$ share the same type of shape, as shown in Fig. 5. From Figs. 5(a) and 5(b), we find that both $|q_1|^2$ and $|q_2|^2$ have one peak and two valleys in each temporal periodic unit. As shown in Figs. 5(c) and 5(d), the Kuznetsov–Ma breather is formed such that the background is accumulated into the central part for each periodic unit. This leads to the generation of a hump with two grooves on the background along the space direction, and the critical peak of the hump can occur in each periodic unit.

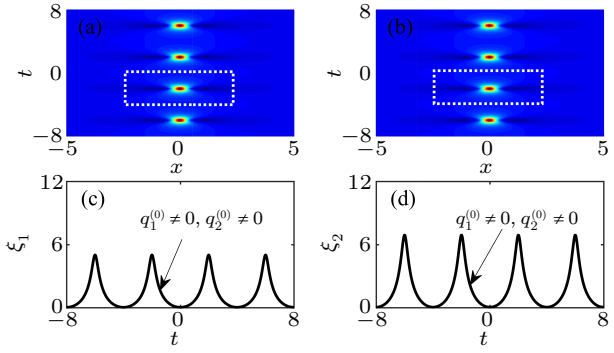


Fig. 5. The transmission of the Kuznetsov–Ma breather solution in Eq. (6): (a) transmission for component $|q_1|^2$ and (b) transmission for component $|q_2|^2$. A notable feature is that they share the same type of shape, and they both have one peak and two valleys in each temporal periodic unit. The nonuniform exchange in Eq. (8) is shown in (c) for ξ_1 and in (d) for ξ_2. The parameters are $\nu = 1$, $C_1 = 1$, $C_2 = 0.65$, $C_3 = C_4 = 0$, $a_1 = 0.5965$, and $a_2 = 0.7$.

4. Exact asymmetric Akhmediev breather solutions

When $\nu^2 < a_1^2 + a_2^2$, equation (1) admits the Akhmediev breather solutions in Eq. (6), which is characterized by the key parameters

$$\Xi = \mathrm{i}\xi,\ \xi = \sqrt{(a_1^2 + a_2^2) - \nu^2},$$
$$A \equiv \theta + \mathrm{i}\varphi = -2\nu t\xi + \mathrm{i}x\xi. \tag{9}$$

The above parameters mean that the main characteristic properties of Akhmediev breather solutions in Eq. (6) with the parameters in Eqs. (4) and (9) are temporally aperiodic and spatially periodic.

The Akhmediev breather solutions can almost exactly describe the modulation instability in nonlinear physics, which is characterized by the periodic energy exchange between a perturbation and a cw background. This process can be used to generate the high-repetition-rate pulse trains in optical fibers.[61] In optical fibers, the temporal periodic property of Akhmediev breathers[62] denotes a single growth–return cycle in the propagation direction, namely a visual illustration of the famous Fermi–Pasta–Ulam recurrence.[63–65] Recently, modulation instability has been found to play a central role in the emergence of highly localized rogue wave structures in various contexts of nonlinear physics. It is obvious that the shape type of Akhmediev breather solutions can be affected by choosing the parameters C_j, and we will discuss the Akhmediev breather solutions in the same way as the Kuznetsov–Ma breather solutions.

For simplicity, we consider the case of $C_2 = 0$, and give the graphical illustration of density distribution for the components q_1 and q_2 in Fig. 6 for the single and two seed solutions, respectively. From Figs. 6(a) and 6(d), we observe that the single seed solution ($q_1^{(0)} \neq 0$, $q_2^{(0)} = 0$) can cause a dark Akhmediev breather with six valleys for its own component q_1 in each temporal periodic unit, while the other component q_2 has the graphical image of bright Akhmediev breather solutions with four peaks, and vice versa (Figs. 6(b) and 6(e)). The unit period can be affected by the amplitude a_2. It is interesting to point out that the graphical illustration of q_1 in each periodic unit seemingly forms two craters. For the existence of two seed solutions, we find that both $|q_1|^2$ and $|q_2|^2$ have four peaks and two valleys in each periodic unit, as shown in Figs. 6(c) and 6(f).

Furthermore, if one considers the case of $C_2 = C_3 = 0$, the density distribution of q_1 and q_2 is plotted in Fig. 7 for the single and two seed solutions, respectively. From Figs. 7(a) and 7(d), we see that under the effect of the single seed solution ($q_1^{(0)} \neq 0$, $q_2^{(0)} = 0$), the component q_1 has four valleys in each temporal periodic unit, while the other component q_2 has the graphical image of bright Akhmediev breather solutions with two peaks and two valleys, and vice versa (Figs. 7(b) and 7(e)). For the existence of two seed solutions, we find that $|q_1|^2$ and $|q_2|^2$ take the same periodic change with the alternate peak and valley in each periodic unit, as shown in Figs. 7(c) and 7(f).

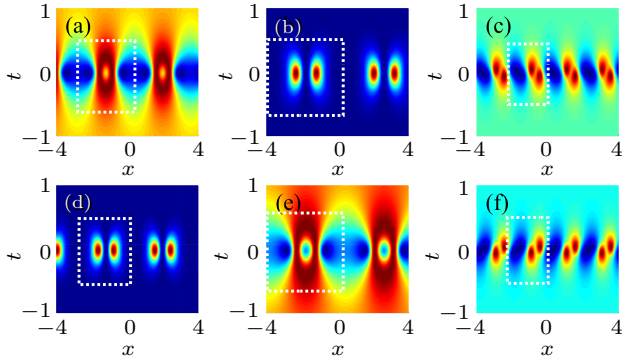


Fig. 6. The dynamic evolution of the Akhmediev breather solution in Eq. (6) with the parameters $\nu = 1$, $C_1 = C_3 = 1$, $C_2 = 0$, and $C_4 = 1.5$. (a)–(c) Dynamic evolutions for the component $|q_1|^2$, and (d)–(f) dynamic evolutions for the component $|q_2|^2$. It can be seen that both (a) and (e) are dark Akhmediev breathers, both (b) and (d) are bright Akhmediev breathers, and (c) and (f) possess two peaks and one valley in each periodic unit. Other parameters are as follows: (a) and (d) $a_1 = 1.4$, $a_2 = 0$; (b) and (e) $a_1 = 0$, $a_2 = 1.2277$; (c) and (f) $a_1 = 1.4$, $a_2 = 1.2277$.

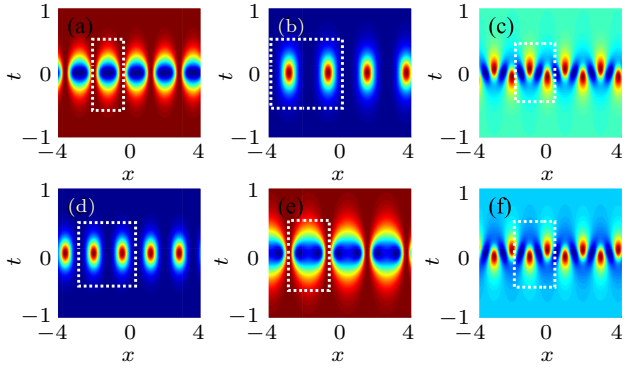


Fig. 7. The dynamic evolution of the Akhmediev breather solution in Eq. (6) with the parameters $\nu = 1$, $C_1 = 1$, $C_2 = C_3 = 0$, and $C_4 = 1$. (a)–(c) Dynamic evolution for component $|q_1|^2$, and (d)–(f) dynamic evolution for component $|q_2|^2$. Other parameters are as follows: (a) and (d) $a_1 = 1.4$, $a_2 = 0$; (b) and (e) $a_1 = 0$, $a_2 = 1.2277$; (c) and (f) $a_1 = 1.4$, $a_2 = 1.2277$.

5. Rogue wave solution

From the above two sections, we see that there is a critical condition $\nu^2 = a_1^2 + a_2^2$ that divides the modulation instability process and the periodization process. This leads to a different physical behavior, i.e. how the breather characteristics depend on the modulation parameter ν. It should be noted that this very interesting phenomenon occurs only under the limitation of $\nu^2 \to a_1^2 + a_2^2$ and the conditions of $C_1 = -C_2$ and $C_3 = -C_4$. Two different asymptotic behaviors are plotted in Figs. 8 and 9 in the limit processes $|\nu| \to \left(\sqrt{a_1^2 + a_2^2}\right)^+$ and $\left(\sqrt{a_1^2 + a_2^2}\right)^-$ under the conditions $C_1 = -C_2$ and $C_3 = -C_4$, respectively. The former case demonstrates a spatial periodic process of the Kuznetsov–Ma soliton forming one hump and two grooves,

and the other case shows the time periodic process of forming the Akhmediev breather. As the modulation parameter $|\nu|$ approaches $\sqrt{a_1^2+a_2^2}$, the spatial and temporal separation of adjacent peaks gradually increases. Finally, the critical state changes from the spatial and temporal periodic process to a localized process of the cw background, i.e. rogue wave solutions.

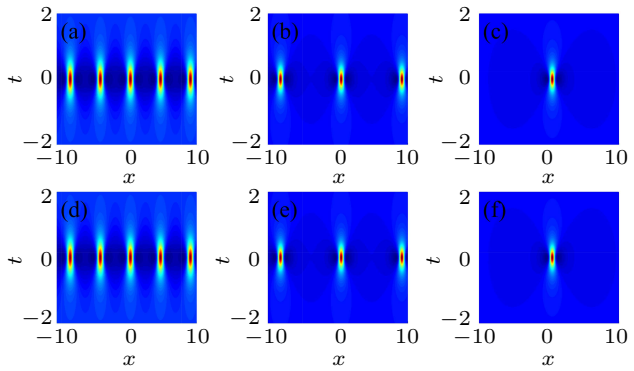


Fig. 8. A sketched demonstration of the density plot in the limit $|\nu| \to \left(\sqrt{a_1^2+a_2^2}\right)^-$ in Akhmediev breather solution using Eq. (6) with $C_1=-1$, $C_2=1$, $C_3=3$, $C_4=-3$, $a_1=0.8$, and $a_2=0.7$. Note that there is one peak and two caves in each periodic. (a)–(c) Density plots for component $|q_1|^2$, and (d)–(f) density plots for component $|q_2|^2$. The modulation parameter ν of the Akhmediev breather is as follows: (a) and (d) $\nu=0.7746$; (b) and (e) $\nu=1$; (c) and (f) $\nu=1.063$.

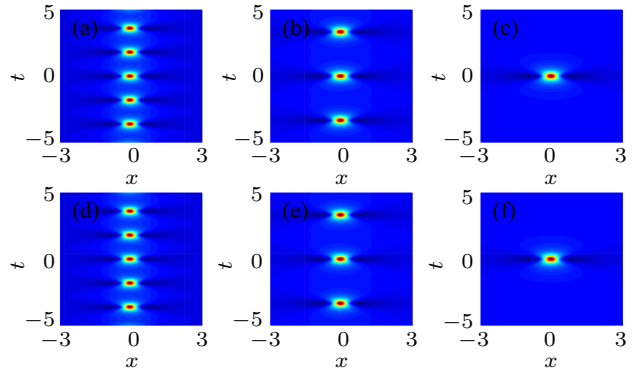


Fig. 9. A sketched demonstration for the limit case $|\nu| \to \left(\sqrt{a_1^2+a_2^2}\right)^+$ in Kuznetsov–Ma breather solution using Eq. (6) with $C_1=-1$, $C_2=1$, $C_3=3$, $C_4=-3$, $a_1=0.8$, and $a_2=0.7$. Note that there is also one peak and two caves in each periodic unit. (a)–(c) For component $|q_1|^2$, and (d)–(f) for component $|q_2|^2$. The modulation parameter ν of the Kuznetsov–Ma breather is as follows: (a) and (d) $\nu=1.2649$; (b) and (e) $\nu=1.1401$; (c) and (f) $\nu=1.063$.

The formation mechanism of the rogue wave is explained in Figs. 10(a) and 10(b). From Fig. 10, we find that as the modulation parameter $|\nu|$ approaches $\sqrt{a_1^2+a_2^2}$, the total nonuniform exchange gradually increases, while the period of total nonuniform exchange goes up. Finally, the total exchange forms the local property. The energy and particles in the background accumulate to the central part when $t<0$. This leads to the generation of a hump with two grooves on the background along the space direction. In contrast, when $t>0$, the rogue waves in the hump start to dissipate into the background so that the hump gradually decays. The rogue wave ultimately disappears, which verifies that the rogue wave is only one oscillation in temporal localization and displays an unstable dynamic behavior, as shown in Figs. 8(c), 8(f), 9(c), and 9(f).

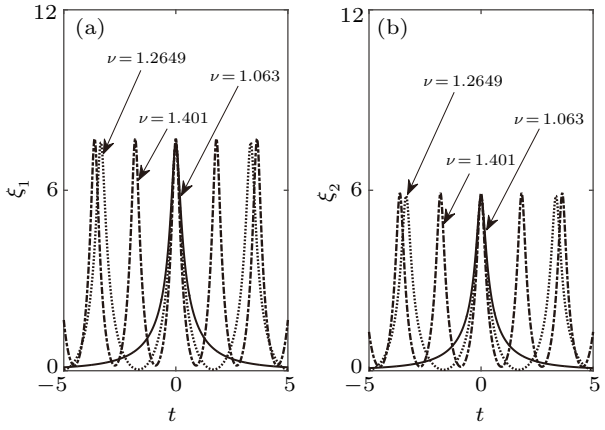


Fig. 10. The nonuniform exchange of the transformation from the Kuznetsov–Ma breather solution to rogue waves in Eq. (8): (a) For ξ_1 and (b) for ξ_2. The parameters are $C_1=-1$, $C_2=1$, $C_3=3$, $C_4=-3$, $a_1=0.8$, and $a_2=0.7$; $\nu=1.2649$ (short dashed line); $\nu=1.1401$ (long dashed line); $\nu=1.063$ (solid line).

6. Conclusion

In this paper, based on the developed Darboux transformation method, we give some types of exact breather and rogue wave solutions in CNLS equations, which can be used to describe transition dynamics of a one-dimensional or two-component Bose–Einstein condensate system with particle transition in strong interaction regimes and other nonlinear systems. We mainly investigate Kuznetsov–Ma breather solutions, Akhmediev breather solutions, and rogue wave solutions. The total nonuniform exchange is also studied in detail. These studies not only lay a theoretical foundation for the study of physics and nonlinear science, but also provide new ideas for the analysis and control of complex systems.

References

[1] Hasegawa A and Tappert F 1973 *Appl. Phys. Lett.* **23** 142
[2] Ablowitz M J and Musslimani Z H 2013 *Phys. Rev. Lett.* **110** 064105
[3] Sulem C and Sulem P 1993 *Appl. Math. Sci.* **3** 102
[4] Bergé L 1998 *Phys. Rep.* **303** 259
[5] Malomed B A, Mihalache D, Wise F and Torner L 2005 *J. Opt. B: Quantum Semiclassical Opt.* **7** R53
[6] Chabchoub A, Hoffmann N P and Akhmediev N 2011 *Phys. Rev. Lett.* **106** 204502
[7] Chabchoub A, Hoffmann N P and Akhmediev N 2012 *J. Geophys. Res.* **117** C00J03
[8] Chabchoub A, Hoffmann N, Onorato M and Akhmediev N 2012 *Phys. Rev. X* **2** 011015
[9] Akhmediev N and Pelinovsky E 2010 *Eur. Phys. J. Spec. Top.* **185** 1
[10] Pelinovsky E and Kharif C 2008 *Extreme Ocean Waves* (Berlin: Springer)
[11] Pitaevskii L and Stringari S 2016 *Bose–Einstein Condensation and Superfluidity* (Oxford: Oxford University Press)
[12] Zakharov V E and Shabat A B 1971 *Zh. Eksp. Teor. Fiz* **61** 118
[13] Bailung H and Nakamura Y 1993 *J. Plasma Phys.* **50** 231
[14] Ruderman M S 2010 *Eur. Phys. J. Spec. Top.* **185** 57

[15] Moslem W M, Shukla P K and Eliasson B 2011 *Euro. Phys. Lett.* **96** 25002
[16] Zeba I, Yahia M E, Shukla P K and Moslem W M 2012 *Phys. Lett. A* **376** 2309
[17] Kibler B, Fatome J, Finot C, Millot G, Genty G, Wetzel B, Akhmediev N, Dias F and Dudley J M 2012 *Sci. Rep.* **2** 463
[18] Zhao F, Li Z D, Li Q Y, Wen L, Fu G S and Liu W M 2012 *Ann. Phys.* **327** 2085
[19] Li Z D, Li Q Y, Xu T F and He P B 2016 *Phys. Rev. E* **94** 042220
[20] Li Z D, Li Q Y and Liu W M 2017 *J. Phys.: Conf. Ser.* **827** 012002
[21] He P B, Gu G N and Pan A L 2012 *Eur. Phys. J. B* **85** 119
[22] Li Q Y, Zhao F, He P B and Li Z D 2015 *Chin. Phys. B* **24** 037508
[23] Li Z D, Cui H, Li Q Y and He P B 2018 *Ann. Phys.* **388** 390
[24] Yan Z 2010 *Commun. Theor. Phys.* **54** 947
[25] Yan Z 2011 *Phys. Lett. A* **375** 4274
[26] Yan Z and Dai C 2013 *J. Opt.* **15** 064012
[27] Yan Z 2015 *Appl. Math. Lett.* **47** 61
[28] Yan Z 2016 *Appl. Math. Lett.* **62** 101
[29] Yan Z 2017 *Chaos* **27** 053117
[30] Wen Z and Yan Z 2017 *Chaos* **27** 033118
[31] Zhang G, Yan Z, Wen X Y and Chen Y 2017 *Phys. Rev. E* **95** 042201
[32] Manakov S V 1974 *Sov. Phys. JETP* **38** 248
[33] Baronio F, Degasperis A, Conforti M and Wabnitz S 2012 *Phys. Rev. Lett.* **109** 044102
[34] Zhao L C and Liu J 2012 *J. Opt. Soc. Am. B* **29** 3119
[35] Ling L and Liu Q P 2010 *J. Phys. A* **43** 434023
[36] Ling L, Zhao L C and Guo B 2016 *Commun. Nonlinear Sci. Numer. Simul.* **32** 285
[37] Ling L, Zhao L C and Guo B 2015 *Nonlinearity* **28** 3243
[38] Zhao L C, Ling L, Yang Z Y and Liu J 2015 *Commun. Nonlinear Sci. Numer. Simul.* **23** 21
[39] Ling L, Feng B F and Zhu Z 2016 *Physica D* **327** 13
[40] Feng B F, Ling L and Zhu Z 2016 *Phys. Rev. E* **93** 052227
[41] Ling L M, Feng B F and Zhu Z N 2018 *Nonlinear Anal. Real World Appl.* **40** 185
[42] Park Q H and Shin H J 2000 *Phys. Rev. E* **61** 3093
[43] Guo B, Ling L and Liu Q P 2013 *Stud. Appl. Math.* **130** 317
[44] Wen X Y, Yang Y and Yan Z 2015 *Phys. Rev. E* **92** 012917
[45] Lü X and Tian B 2012 *Phys. Rev. E* **85** 026117
[46] Kibler B, Fatome J, Finot C, Millot G, Dias F, Genty G, Akhmediev N and Dudley J M 2010 *Nat. Phys.* **6** 790
[47] Yang J K 1997 *Physica D* **108** 92
[48] He J S, Mei J and Li Y S 2007 *Chin. Phys. Lett.* **24** 2157
[49] Dai C Q, Fan Y, Zhou G Q, Zheng J and Chen L 2016 *Nonlinear Dyn.* **86** 999
[50] Liu C, Yang Z Y, Zhao L C and Yang W L 2014 *Phys. Rev. A* **89** 055803
[51] Dudley J M, Genty G, Dias F, Kibler B and Akhmediev N 2009 *Opt. Express* **17** 21497
[52] Karif C and Pelinovsky E 2003 *Eur. J. Mech. B Fluids* **22** 603
[53] Karif C, Pelinovsky E and Slunyaev A 2009 *Rogue Waves in Waters of Infinite and Finite Depths* (Berlin: Springer) p. 91
[54] He J, Xu S and Porsezian K 2012 *Phys. Rev. E* **86** 066603
[55] Ling L and Zhao L C 2015 *Phys. Rev. E* **92** 022924
[56] Guo B and Ling L M 2011 *Chin. Phys. Lett.* **28** 110202
[57] Ankiewicz A, Devine N and Akhmediev N 2009 *Phys. Lett. A* **373** 3997
[58] Ruban V, Kodama Y, Ruderman M, Dudley J, Grimshaw R, McClintock P V E, Onorato M, Kharif C, Pelinovsky E, Soomere T, Lindgren G, Akhmediev N, Slunyaev A, Solli D, Ropers C, Jalali B, Dias F and Osborne A 2010 *Eur. Phys. J. Special Topics* **185** 5
[59] Höhmann R, Kuhl U, Stöckmann H J, Kaplan L and Heller E J 2010 *Phys. Rev. Lett.* **104** 093901
[60] Erkintalo M, Genty G and Dudley J M 2009 *Opt. Lett.* **34** 2468
[61] Hasegawa A 1984 *Opt. Lett.* **9** 288
[62] Akhmediev N N and Korneev V I 1986 *Theor. Math. Phys.* **69** 1089
[63] Akhmediev N N 2001 *Nature* **413** 267
[64] Van S G, Emplit P and Haelterman M 2001 *Phys. Rev. Lett.* **87** 033902
[65] Mussot A, Kudlinski A, Droques M, Szriftgiser P and Akhmediev N 2014 *Phys. Rev. X* **4** 011054